

# Synthesis and Characterization of Carbon Aerogels Electrodes Modified by Ag<sub>2</sub>S Nanoparticles

Ramsés R. García Martínez<sup>a</sup>, Claudia Alejandra Rodríguez González<sup>a</sup> 

Juan Francisco Hernández-Paz<sup>a</sup> , Florinda Jiménez Vega<sup>b</sup> , Héctor Camacho Montes<sup>a</sup> 

Imelda Olivas Armendáriz<sup>a</sup> 

<sup>a</sup>Universidad Autónoma de Ciudad Juárez, Instituto de Ingeniería y Tecnología, Avenida del Charro No. 450 Norte, 32310 Ciudad Juárez, Chihuahua, México

<sup>b</sup>Universidad Autónoma de Ciudad Juárez, Instituto de Ciencias Biomédicas, Avenida Plutarco Elías Calles 1210, 32310 Ciudad Juárez, Chihuahua, México

Received: August 25, 2020; Revised: January 25, 2021; Accepted: February 21, 2021

In this work, electrodes based on carbon aerogels (CA) modified by Ag<sub>2</sub>S nanoparticles (NPs) were synthesized by sputtering and solid-vapor reactions. Nanoparticles were identified as silver sulfide (acanthite phase) and their size was controlled by the sputtering time (5s deposition- 8.65 nm ± 1.74 nm, 7s deposition- 12.78 nm ± 8.53 nm and 45 s deposition- 21.35 nm ± 10.07 nm). It was found that the electrodes properties vary according to the Ag<sub>2</sub>S NPs sizes. All modified electrodes exhibited an improved REDOX reactions reversibility, enhanced optical properties (0.97 to 1.22 eV optical bandgap) and electrical conductivity (8.60-9.40 S/cm) when compared with pure carbon aerogel electrodes (1.4 eV, 8.20 S/cm).

**Keywords:** Carbon aerogel, Ag<sub>2</sub>S nanoparticles, electrodes.

## 1. Introduction

Electrochemical biosensors are sensors that use electrochemical transducers (e.g. glass, metal, carbon electrodes, ion-selective electrodes) for detecting biological material or non-biological matrixes<sup>1</sup>. Despite electrochemical biosensors have existed for more than 60 years, their great potential for future biosensing techniques have been established and several types of electrochemical biosensors have been developed and commercialized for different purposes. This is due to their selective biochemical recognition as well as their high detection sensitivity coupled to their low cost compared with other common techniques as electrochemiluminescence or fluorescence<sup>2,3</sup>. The electrode is a fundamental component of these type of biosensors and it is used a support for biomolecules immobilization and electron transfer. Significant research work is taking place focused on the development of carbon aerogel (CA) electrodes for biosensors<sup>4-10</sup>. Carbon aerogel (CA) are at relatively low cost and they exhibit important properties such as electric double layer performance, porous structures, high surface area and transportation channels for electrolyte ions<sup>4,5,11-16</sup>. These CA electrodes can be modified with different nanoparticles (e.g. Ni, Pd, Ag<sub>2</sub>S, CuS, CdSe, WO<sub>3</sub>, Au, PtNi, NiCo<sub>2</sub>S<sub>4</sub>) to enhance their electrical or electrochemical performance<sup>17-25</sup>. Silver sulfide (Ag<sub>2</sub>S) is an important nontoxic semiconductor recognized for its optical and electrical properties. Currently, different synthesis methodologies have been reported for this compound including, sol-gel, micro-emulsion, microwave, wet chemistry, organic

metallic precursors, sputtering, and solid-vapor reactions. Some of the main challenges during the synthesis process are obtaining a narrow particle size distribution and good dispersion<sup>20,26-30</sup>. In this work, electrodes based on carbon aerogel and Ag<sub>2</sub>S NPs were synthesized by a simple methodology using sputtering and solid-vapor reactions<sup>31</sup>. Low cost, low by-product formation, low processing temperatures, and narrow particle size distribution are advantages of this proposed synthesis methodology.

## 2. Material and Methods

The electrodes based on carbon aerogel modified with Ag<sub>2</sub>S NPs were fabricated cutting 1cm x 1cm samples of carbon aerogel (READE-Grade II). Silver deposition on carbon aerogel was made by sputtering Denton Vacuum Desk-V with a 99.9% silver target from Ted Pella Inc. (P/N 91118). Solid-vapor reactions were used for the synthesis of Ag<sub>2</sub>S NPs on the carbon aerogel electrodes. They were prepared placing 100ml of deionized water, 3g of sublimated sulfur (99.97%, Fermont-PQ09122) and the samples of carbon aerogel with silver in a baker covered by aluminum foil and tape. The baker was placed in an oven Quincy Lab-20-AF for 3 hours at 110 °C to synthesis Ag<sub>2</sub>S NPs. Possible reactions are shown in 1, 2 and 3<sup>31</sup>.



\*e-mail: [claudia.rodriguez@uacj.mx](mailto:claudia.rodriguez@uacj.mx)



Electrodes morphologies, elemental chemical composition and phases were determined by scanning electron microscopy (SEM), energy dispersive X-Ray spectroscopy (EDS) and X-Ray diffraction (XRD). SEM image analysis was performed to determine the NPs size (at least 200 measurements for each sample). A Keithley-2400 source meter was used to characterize electrical properties using a four-point probe method applying a sweep function with a ramp from 0 V to 1 V. A spectrometer with an integrating sphere Stellar Net were used to characterize optical properties. The Kubelka-Munk function was used to estimate the optical band gap energy making use of the diffuse reflectance spectra<sup>32</sup>. A Xenon lamp generates wavelengths from 100 nm to 1000 nm. The bandgap was calculated using the spectra obtained, they were processed in origin software extrapolating the straight-line portion of the curves to zero absorption coefficient to estimate band gap energy of each electrode taking into consideration Kubelka-Munk function (4), used to estimate the optical band gap energy making use of diffuse reflectance spectra<sup>32</sup>.

$$F(R) = \frac{(1-R)^2}{2R} = \frac{k}{s} \quad (4)$$

Where  $F(R)$  is the Kubelka-Munk function,  $R$  is the reflectance data,  $s$  is the scattering factor and  $k$  is the absorption coefficient.

A potentiostat “CorrTest model Cs350” was used to characterize the electrodes by cyclic voltammetry. An electrolyte of potassium ferrocyanide with a support solution of potassium chloride and a potential range from -2.5 V to 2.5 V were used to validate reversibility in the electrochemical reaction and to study redox mechanism.

### 3. Results and Discussion

$Ag_2S$ -CA electrodes were analyzed by SEM, XRD and EDS. NP's were characterized as acanthite phase  $Ag_2S$

(JCPDS#14-0074) which correspond to the equilibrium phase and is in agreement with our previous work<sup>33</sup>. Two broad reflections at approximately  $2\theta$  angle of 23 and  $43^\circ$  were also identified that correspond to the graphitic phase of the carbon aerogel (JCPDS#22-1069). It was observed that NPs size is smaller when the silver deposition time is lower since there is less silver to react with sulfur forming smaller NPs (Figure 1). Two parameters change when silver deposition time is modified: one is NPs uniformity and the other one is the NPs size average. The NPs size, as mentioned before, depends on the amount of silver deposition because of solid-vapor reaction is a bottom-up synthesis method<sup>34</sup>. The sulfidation temperature and time play an important role to modify NPs size through the nucleation and growth process. NPs size and size distribution are parameters that must be considered when a working electrode is designed because when these parameters are modified, their optical and electric properties can be enhanced. Brus et al. found, through the measurement of redox potentials of organic molecules using electrodes of photo-excited semiconductors, that the performance of the electrodes depends on the size and distribution of the NPs<sup>35</sup>.

Moreover, if the NPs size is in the quantum dots (QD) size range (case of 5s silver deposition), the optical properties are produced by the interaction between the plasmon of the surface of the QD and the incident electromagnetic wave occurring a quantum confinement on the electronic structure induced by QD size and shape<sup>36</sup>. Also, QD will act as an efficient immobilization matrix of receptors (antibodies, enzymes, bacteria, among others). Hence, when a working electrode for electrochemical sensors doped with NPs is designed the morphology of the NPs should be uniform and exhibit the smallest possible size<sup>35</sup>. In this case, the electrode with 5 seconds of silver deposition presents greater NPs uniformity and smaller average size than the other samples (Figure 1 and Table 1).

The absorption VIS-NIR radiation also depends on NPs size and size distribution on the electrode, thus, synthesis

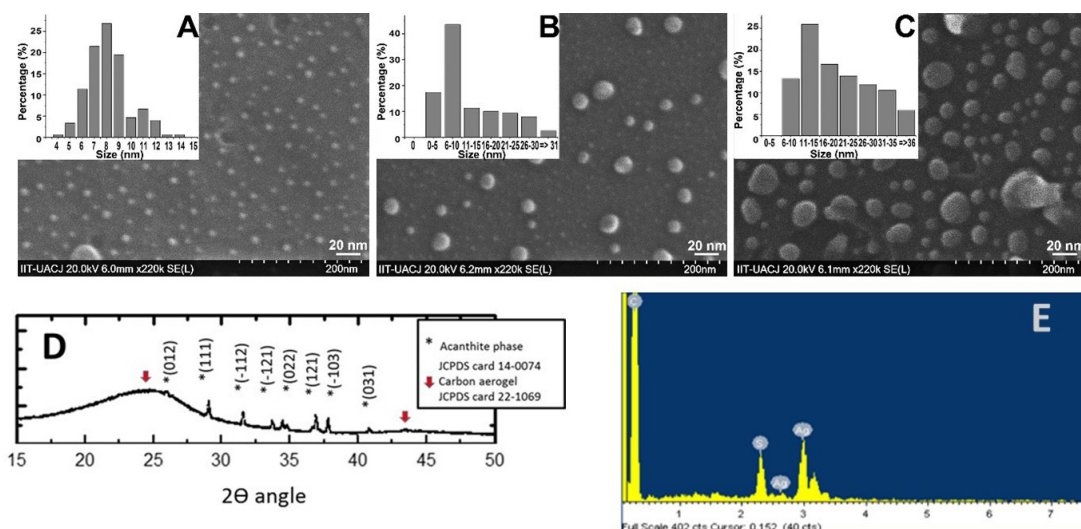


**Figure 1.** SEM images of electrodes based on CA- $Ag_2S$  NPs with different time of silver deposition, A) 5 s, B) 7 s and C) 45 s silver deposition. D) and E) Example of XRD and EDS analyses of the electrodes.

of NPs with narrow size distributions is essential to take advantage of optical properties and quantum confinement<sup>37</sup>. The electrode with 5s of silver deposition presents the maximum absorbance showing the best optical properties compared with the other samples (Figure 2). All samples present a maximum adsorption edge in a wavelength of ~525nm and a bandgap in the range of 0.97 to 1.40 eV which are in agreement to the bandgap values reported for similar systems (1.2- 1.8 eV)<sup>38,39</sup>. The reflectance and bandgap increases when the Ag<sub>2</sub>S nanoparticles agglomeration occurs. On the other hand, the bandgap decreases, when the NPs radius is reduced due to their electronic structure<sup>37</sup>.

Table 2 shows a comparison of the electrical conductivity of the electrodes obtained in this work with the reported values by other researchers for carbon aerogel electrodes with similar densities since it is well known that the electrical conductivity increases with increasing carbon aerogel densities. It can be observed that the electrical conductivity values are between the reported ranges and the Ag<sub>2</sub>S nanoparticles modification of the electrodes increase this value. Figure 3 represents the electric behavior, where it is also shown that the conductivity of carbon aerogel without NPs is lower than in the other samples. It is seen that with more silver deposition time, the electrode compound exhibits a larger conductivity but, as can be observed in optical characterization, if silver deposition time increases their optical properties decrease due to agglomerates of silver sulfide nanoparticles formed on the surface of carbon aerogel. Agglomerations of nanoparticles affect the light absorption but

**Table 1.** Average NPs size and optical band gap of the electrodes.

Time of silver deposition	Average size of Ag <sub>2</sub> S NPs	Optical band gap
A) 0s	-----	1.40eV
B) 5s	8.65nm ± 1.74 nm	0.97eV
C) 7s	12.78nm ± 8.53nm	1.18eV
D) 45s	21.35nm ± 10.07nm	1.22eV

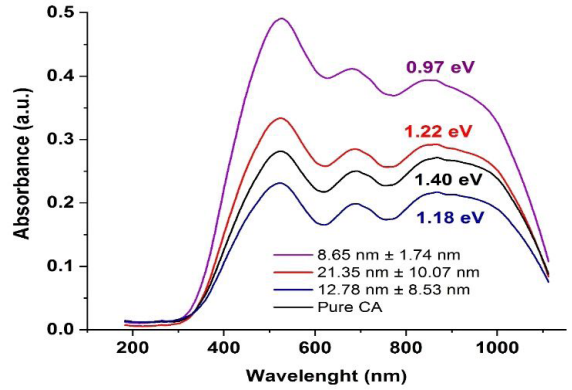


**Figure 2.** UV-VIS absorption spectra of the synthesized electrodes and pure carbon aerogel.

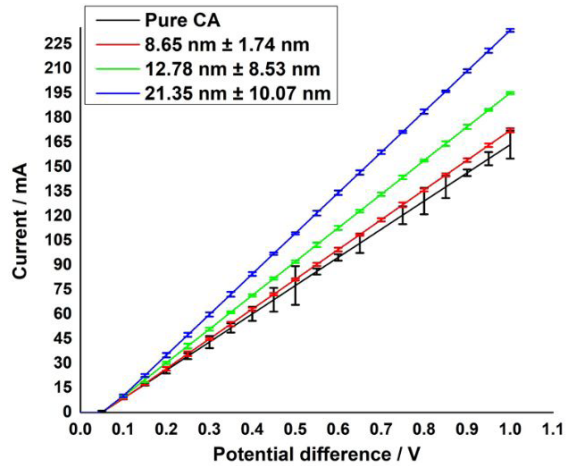


**Figure 3.** I-V curve of the synthesized electrodes and pure carbon aerogel.

**Table 2.** Comparison of carbon aerogel densities and electrical conductivities.

Sample	Density (g cm <sup>-3</sup> )	Electrical conductivity (S / cm)	Reference
Pristine carbon aerogel	0.15	2.27	41
Carbon aerogels via pyrolyzing (700-1100oC) resorcinol–formaldehyde (RF)	0.14-0.18	0.4-0.46	42
Carbon aerogel resorcinol–formaldehyde (Supercritical fluid drying and carbonization)	0.1-0.4	1.5-11.75	43
Carbon aerogels via pyrolyzing resorcinol–formaldehyde (RF) (Modified ambient dried technique)	0.45-0.85	5.80-15.84	44
RF (resorcinol formaldehyde) organic aerogels	0.50	13.2	45
Pristine carbon aerogel (Reade grade II via pyrolyzing resorcinol–formaldehyde*)	0.4 *	8.20	This work
Carbon aerogel (Reade grade II via pyrolyzing resorcinol–formaldehyde*) with Ag <sub>2</sub> S nanoparticles (8.65 nm ± 1.74 nm)	0.4 *	8.60	This work
Carbon aerogel (Reade grade II via pyrolyzing resorcinol–formaldehyde*) with Ag <sub>2</sub> S nanoparticles (12.78 nm ± 8.53)	0.4*	8.60	This work
Carbon aerogel (Reade grade II via pyrolyzing resorcinol–formaldehyde*) with Ag <sub>2</sub> S nanoparticles (21.35 nm ± 10.07)	0.4*	9.40	This work

\*Information according to the supplier (Reade grade II).

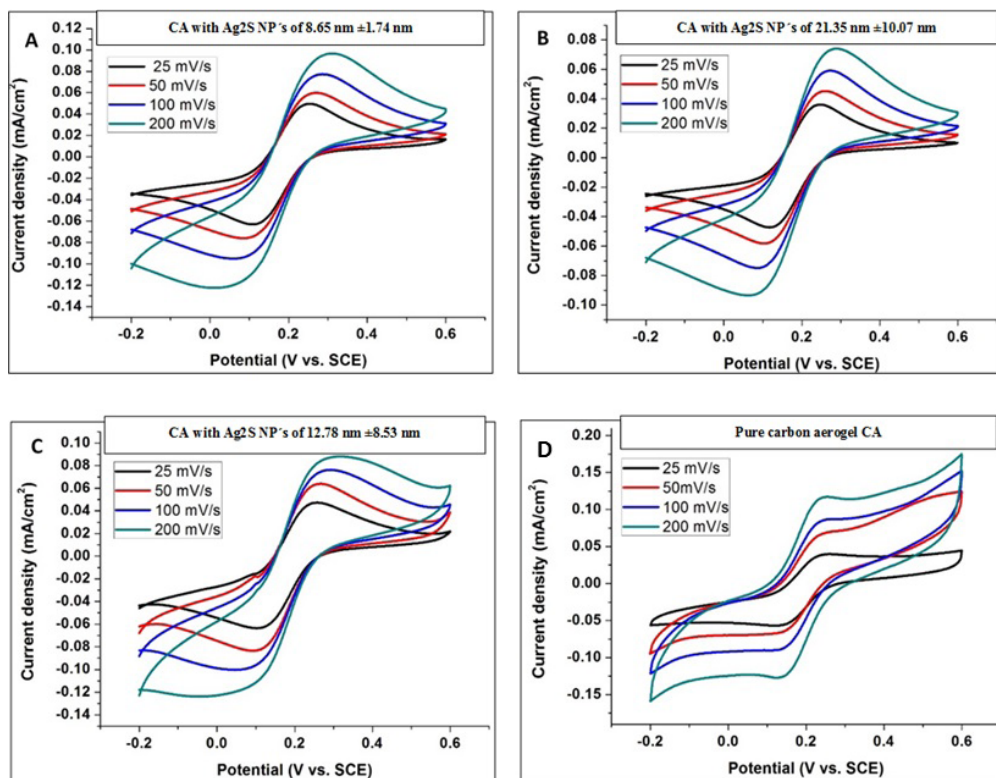


Figure 4. Cyclic voltammetry of the synthesized electrodes and pure carbon aerogel.

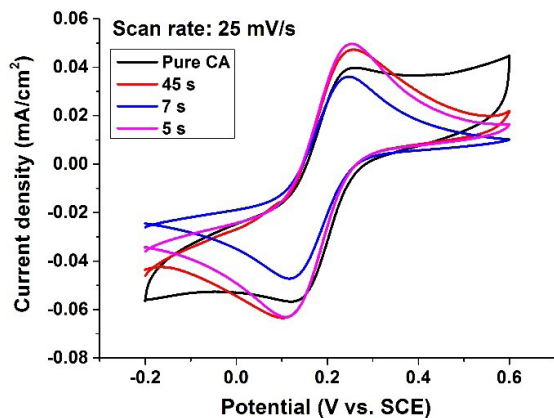


Figure 5. Comparison of the synthesized electrodes and pure carbon aerogel voltammograms at a scan rate of 25 mV/s.

improve the electric conductivity of electrodes<sup>40</sup>. All samples maintained a lineal relation because of voltage is directly proportional to the electric current intensity and resistance has not variations because always a constant temperature was kept.

Figures 4A, 4B, 4C, and 4D show the voltammograms of electrodes of pure carbon aerogel and the electrodes with NPs size of 8.65nm  $\pm$  1.74 nm, 12.78nm  $\pm$  8.53nm and 21.35nm  $\pm$  10.07nm, respectively. The modified electrodes with NPs voltammograms show isopoints (crossing points of the voltammograms at different scan rate), good reversibility in redox reactions, and peaks intensity proportional to scan rate. In the pure carbon aerogel case, a capacitive effect is

observed, the redox reactions are not favorable and there is not isopoint presence. Figure 5 shows a comparison of the different electrodes at 25 mV/s scan rate where the voltammograms shape difference between the pure aerogel and the NPs modified electrodes is evident. The behavior shown by the electrodes proved that Ag<sub>2</sub>S NPs improve electron transfer and confers good electrochemical properties as reported by other research works where carbon aerogel and NPs have been used<sup>40</sup>.

## 4. Conclusions

CA electrodes with Ag<sub>2</sub>S NPs have been successfully prepared by a simple solid-vapor reaction technique. The average Ag<sub>2</sub>S NPs size are in the range of 8.65nm to 21.35nm. The Ag<sub>2</sub>S NPs on carbon aerogel increase the absorption of visible and near-infrared light, improve electric conductivity and REDOX reactions reversibility. If Ag<sub>2</sub>S agglomerated nanoparticles are present, the optical properties are largely affected. The electrode with the best optical and electrical properties was obtained with  $\sim$ 5s of silver deposition on carbon aerogel. It showed a homogeneous morphology of Ag<sub>2</sub>S with an average size of NPs of 8.65nm  $\pm$  1.74nm, a bandgap reduction of 30.7% and an electric conductivity increment of 12.7% compared to the pure carbon aerogel electrodes. Cyclic voltammetry analysis shows that these electrodes could be successfully used for electrochemical sensors.

## 5. Acknowledgements

The authors thank CONACYT for the financial support of this project [Grant No. 286011].

## 6. References

1. Thevenot DR, Toth K, Durst RA, Wilson GS. Electrochemical biosensors: recommended definitions and classification. *Pure Appl Chem.* 1999;71(12):2333-48.
2. Grieshaber D, MacKenzie R, Vörös J, Reimhult E. Electrochemical biosensors—sensor principles and architectures. *Sensors (Basel).* 2008;8(3):1400-58.
3. Cho IH, Kim DH, Park S. Electrochemical biosensors: perspective on functional nanomaterials for on-site analysis. *Biomater Res.* 2020;24(1):1-12.
4. Pierre AC, Pajonk GM. Chemistry of aerogels and their applications. *Chem Rev.* 2002;102(11):4243-66.
5. Tewari S. Carbon aerogel electrodes: Adsorption-desorption and regeneration study for purification of water. Texas: Texas Water Resources Institute, 2006. p. 2005-6.
6. Feng S, Yu L, Yan M, Ye J, Huang J, Yang X. Holey nitrogen-doped graphene aerogel for simultaneously electrochemical determination of ascorbic acid, dopamine and uric acid. *Talanta.* 2020;224:121851.
7. Avan AA, Filik H. Simultaneous electrochemical sensing of dihydroxybenzene isomers at multi-walled carbon nanotubes aerogel/gold nanoparticles modified graphene screen-printed electrode. *J Electroanal Chem.* 2020;878:114682.
8. Xie P, Sun W, Liu Y, Du A, Zhang Z, Wu G, et al. 3D Porous Graphene Aerogel@ GOx Based Microfluidic Biosensor for Electrochemical Glucose Detection. *Analyst (Lond).* 2020;145:5141-7.
9. Zhu P, Li S, Zhou S, Ren N, Ge S, Zhang Y, et al. In situ grown COFs on 3D strutted graphene aerogel for electrochemical detection of NO released from living cells. *Chem Eng J.* 2020;In Press:127559.
10. Wang S, Guo P, Ma G, Wei J, Wang Z, Cui L, et al. Three-dimensional hierarchical mesoporous carbon for regenerative electrochemical dopamine sensor. *Electrochim Acta.* 2020;360:137016.
11. Sarapuu A, Kreek K, Kisand K, Kook M. Electrocatalysis of oxygen reduction by iron-containing nitrogen-doped carbon aerogels in alkaline solution. *Electrochim Acta.* 2017;230:81-8.
12. Li F, Ahmad A, Xie L, Sun G, Kong Q, Su F, et al. Phosphorus-modified porous carbon aerogel microspheres as high volumetric energy density electrode for supercapacitor. *Electrochim Acta.* 2019;318:151-60.
13. Zhang X, Zhao J, He X, Li Q, Ao C, Xia T, et al. Mechanically robust and highly compressible electrochemical supercapacitors from nitrogen-doped carbon aerogels. *Carbon.* 2018;127:236-44.
14. Jiang F, He Z, Guo D, Zhou X. Carbon aerogel modified graphite felt as advanced electrodes for vanadium redox flow batteries. *J Power Sources.* 2019;440:227114.
15. Thirumalraj B, Rajkumar C, Chen SM, Veerakumar P, Perumal P, Liu SB. Carbon aerogel supported palladium-ruthenium nanoparticles for electrochemical sensing and catalytic reduction of food dye. *Sens Actuators B Chem.* 2018;257:48-59.
16. Yang I, Kwon D, Kim MS, Jung JC. A comparative study of activated carbon aerogel and commercial activated carbons as electrode materials for organic electric double-layer capacitors. *Carbon.* 2018;132:503-11.
17. Li X, Hu K, Tang R, Zhao K, Ding Y, Li X, et al. CuS quantum dot modified carbon aerogel as an immobilizer for lithium polysulfides for high-performance lithium-sulfur batteries. *RSC Advances.* 2016;6(75):71319-27.
18. Hu H, Wei W, Jiang Z, Sun W, Lv X, Xie J, et al. In situ formation of small-scale Ag<sub>2</sub>S nanoparticles in carbonaceous aerogel for enhanced photodegradation performance. *J Mol Liq.* 2019;292:111476.
19. Arachchige IU, Brock SL. Sol-gel assembly of CdSe nanoparticles to form porous aerogel networks. *J Am Chem Soc.* 2006;128(24):7964-71.
20. Dong S, Li N, Suo G, Huang T. Carbon aerogel supported palladium-ruthenium nanoparticles for electrochemical sensing and catalytic reduction of food dye. *Anal Chem.* 2013;85(24):11739-46.
21. Rajkumar C, Veerakumar P, Chen SM, Thirumalraj B, Liu SB. Facile and novel synthesis of palladium nanoparticles supported on a carbon aerogel for ultrasensitive electrochemical sensing of biomolecules. *Nanoscale.* 2017;9(19):6486-96.
22. Liu X, Sheng G, Zhong M, Zhou X. Dispersed and size-selected WO<sub>3</sub> nanoparticles in carbon aerogel for supercapacitor applications. *Mater Des.* 2018;141:220-9.
23. Wang Y, Zou L, Huang Q, Zou Z, Yang H. 3D carbon aerogel-supported PtNi intermetallic nanoparticles with high metal loading as a durable oxygen reduction electrocatalyst. *Int J Hydrogen Energy.* 2017;42(43):26695-703.
24. Dong J, Li S, Ding Y. Anchoring nickel-cobalt sulfide nanoparticles on carbon aerogel derived from waste watermelon rind for high-performance asymmetric supercapacitors. *J Alloys Compd.* 2020;845:155701.
25. Rajkumar C, Nehru R, Chen SM, Kim H, Arumugam S, Sankar R. Electrosynthesis of carbon aerogel-modified AuNPs@ quercetin via an environmentally benign method for hydrazine (HZ) and hydroxylamine (HA) detection. *New J Chem.* 2020;44(2):586-95.
26. Fike DA, Houghton JL, Moore SE, Gilhooly WP 3rd, Dawson KS, Druschel GK, et al. Spatially resolved capture of hydrogen sulfide from the water column and sedimentary pore waters for abundance and stable isotopic analysis. *Mar Chem.* 2017;2017(197):26-37.
27. Liu Y, Geng P, Wang J, Yang Z, Lu H, Hai J, et al. In-situ ion-exchange synthesis Ag<sub>2</sub>S modified SnS<sub>2</sub> nanosheets toward highly photocurrent response and photocatalytic activity. *J Colloid Interface Sci.* 2018;512:784-91.
28. Sadovnikov SI, Kozlova EA, Gerasimov EY. Photocatalytic hydrogen evolution from aqueous solutions on nanostructured Ag<sub>2</sub>S and Ag<sub>2</sub>S/Ag. *Catal Commun.* 2017;100:178-82.
29. Alshetri BM, Shkir M, Bawazeer TM, AlFaify S, Hamdy MS. A rapid microwave synthesis of Ag<sub>2</sub>S nanoparticles and their photocatalytic performance under UV and visible light illumination for water treatment applications. *Physica E.* 2020;121:114060.
30. Rempel SV, Kuznetsova YV, Rempel AA. Self-Assembly of Ag<sub>2</sub>S Colloidal Nanoparticles Stabilized by MPS in Water Solution. *ACS Omega.* 2020;5(27):16826-32.
31. Duarte-Fierro E, Olivas-Armendariz I, Hernández Paz JF, Rodríguez-González CA, García-Martínez RR, Soto-Rosales HA. *Mexican patent Mx/a/2019/011019.* 2019.
32. Kubelka P. New contributions to the optics of intensely light-scattering materials. Part I. *Josa.* 1948;38(5):448-57.
33. Díaz M, Ramos-Murillo M, Galindo JE, Enríquez-Carrejo JL, Montes H, Hernández-Paz JF, et al. Absorbance and current-voltage hysteresis curve of silver sulfide thin films synthesized by solid-vapor reactions. *Chalco-genide Lett.* 2016;13(5):201-6.
34. Steigerwald ML, Alivisatos AP, Gibson JM, Harris TD, Kortan R, Muller AJ, et al. Surface derivatization and isolation of semiconductor cluster molecules. *J Am Chem Soc.* 1988;110(10):3046-50.
35. Gryczynski I, Malicka J, Jiang W, Fischer H, Warren C, Chan W. Surface-plasmon-coupled emission of quantum dots. *Chem. Phys. B.* 2005;109(3):1088-93.
36. Tubtintae A, Wu KL, Tung HY. Ag<sub>2</sub>S quantum dot-sensitized solar cells. *Electrochem Commun.* 2010;12:1158-60.
37. Lakshminarasimhan N, Kim W, Choi W. Effect of the agglomerated state on the photocatalytic hydrogen production with in situ agglomeration of colloidal TiO<sub>2</sub> nanoparticles. *J Phys Chem C.* 2008;112(51):20451-7.
38. Hu H, Wei W, Jiang Z, Sun W, Lv X, Xie J. In situ formation of small-scale Ag<sub>2</sub>S nanoparticles in carbonaceous aerogel

- for enhanced photodegradation performance. *J Mol Liq.* 2019;292:111476.
39. Wu Q, Zhou M, Gong Y, Li Q, Yang M, Yang Q, et al. Three-dimensional bandgap-tuned Ag<sub>2</sub>S quantum dots/reduced graphene oxide composites with enhanced adsorption and photocatalysis under visible light. *Catal Sci Technol.* 2018;8(20):5225-35.
  40. Peng L, Dong S, Li N, Suo G, Huang T. Construction of a biocompatible system of hemoglobin based on AuNPs-carbon aerogel and ionic liquid for amperometric. *Sens Actuators B Chem.* 2015;210:418-24.
  41. Ahmad Y, Berthon-Fabry S, Chatenet M, Monier G, Dubois M, Guerin K. Advances in tailoring the water content in porous carbon aerogels using RT-pulsed fluorination. *J Fluor Chem.* 2020;238:109633.
  42. Malkova AN, Sipyagina NA, Gozhikova IO, Dobrovolsky YA, Konev DV, Baranchikov AE, et al. Electrochemical properties of carbon aerogel electrodes: dependence on synthesis temperature. *Molecules.* 2019;24(21):3847.
  43. Xie P, Sun W, Liu Y, Du A, Zhang Z, Wu G, et al. Carbon aerogels towards new candidates for double negative metamaterials of low density. *Carbon.* 2018;129:598-606.
  44. Hwang SW, Hyun SH. Capacitance control of carbon aerogel electrodes. *J Non-Cryst Solids.* 2004;347(1-3):238-45.
  45. Jung HH, Hwang SW, Hyun SH, Lee KH, Kim GT. Capacitive deionization characteristics of nanostructured carbon aerogel electrodes synthesized via ambient drying. *Desalination.* 2007;216(1-3):377-85.